Analysis of misty plasma processes using a new multisource reactor allowing for *in plasma* surface characterization

S. Chouteau[1,2], A. Granier[2], M. Richard-Plouet[2] and L. Stafford[1]

[1] *Département de physique, Université de Montréal, Montréal, Québec, Canada*
[2] *Nantes Université, CNRS, Institut des Matériaux de Nantes Jean Rouxel, IMN, Nantes, France*

Abstract: Misty plasma processes have gained significant interest due to their capacity to manufacture (multi)functional thin films. However, nanoparticles tend to accumulate in micrometer-scale ring-like structures ('coffee ring' effect) in such processes. The possible roles played by substrate heating and plasma-droplet interactions on the nanoparticles' supply and spatial organization is examined using a multisource reactor with *in plasma* surface characterization.

Keywords: misty plasma, nanocomposite, thin films, droplet, coffee ring effect

1. Introduction

Over the past years, the search for multifunctional nanocomposite thin films has led to the development of multiple strategies involving plasma processes. Recently, the injection of liquid colloidal solutions in plasma deposition systems as a direct supply of pre-formed nanoparticles has shown promising results. In these hybrid sol-gel/plasma experiments, suspensions are sprayed into the plasma as aerosols during matrix deposition [1]. Literature related to this "misty plasma" approach is now growing steadily for atmospheric-pressure processes, but is still rather tentative for low-pressure reactors.

In this context, we recently developed a low-pressure misty plasma system for the growth of inorganic-matrix nanocomposite thin films [2,3]. Although coatings exhibited high nanoparticle content and decent optical properties, nanoparticles tended to accumulate in micrometer-scale ring-like structures [2]. Recent examples of structures obtained in low-pressure misty plasmas with TiO_2 nanoparticles dispersed in a SiO_2 matrix are provided in Figure 1. This phenomenon, commonly referred to as the 'coffee ring' effect, is emblematic of evaporating colloidal droplets. Also shown in Fig. 1 is a corresponding map of the nanoparticles' Raman signal intensity (TiO_2 anatase peak at 154 cm^{-1}). From this comparison, it is clear that the optical images describe accurately the distribution of nanoparticles.

The role played by the reactive plasma environment in the formation of these structures is unknown. The ambition of the multisource experiment presented here is the unveilment of synergetic effects in misty plasma processes leading to the aforementioned self-organized nanoparticles clusters. The present work is a first step towards this objective.

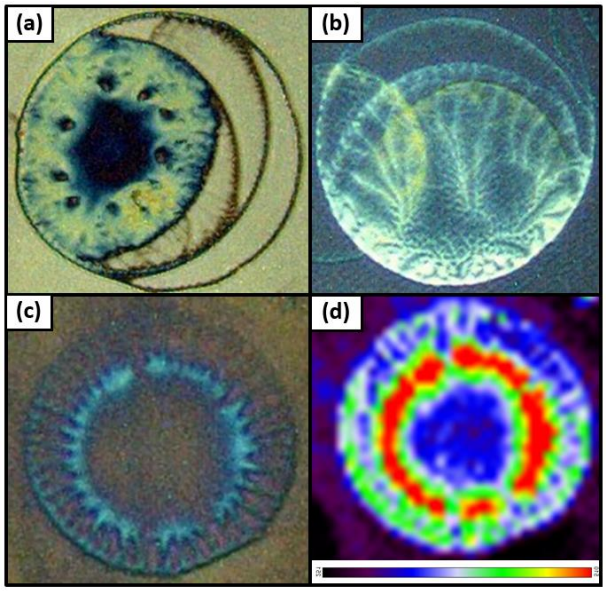

Figure 1 – Typical optical micrographs of coffee rings as seen on nanocomposite films in the misty plasma experiment, with diameters of (a) 110 µm, (b) 40 µm, (c) 15 µm. (d) TiO_2 Raman intensity map of the last droplet imprint.

2. Experimental details

A simplified diagram of the multisource reactor used in this experiment is shown in Figure 2. It consists of a 36 cm-diameter stainless steel vacuum chamber on which are mounted three identical ICP radiofrequency plasma sources. Two of these sources contain a set of metal grids to which a voltage can be applied to produce ion beams of controlled energy.

The vacuum chamber is situated at the end of a 2 MeV Tandetron accelerator beam line, which allows for *in plasma* surface analysis using ion beam diagnostics, namely Rutherford backscattering spectroscopy (RBS) and elastic recoil detection (ERD). A 532 nm laser and a spectrometer are also available for *in plasma* Raman spectroscopy measurements.

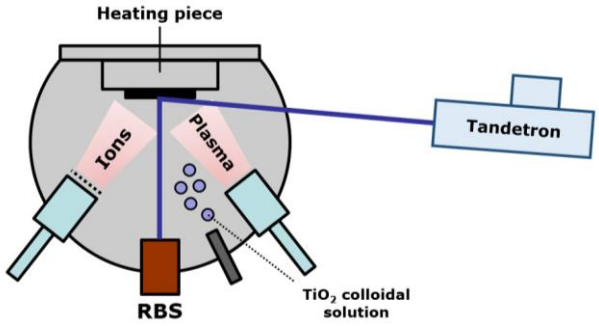

Figure 2 – Simplified diagram of the multisource reactor equipped with *in plasma* surface analysis.

A Kemstream liquid doser was used to inject pulses of a colloidal solution of TiO_2 nanoparticles suspended in a solvent mixture of methanol, propylene glycol, propylene carbonate (volume fraction of 25:55:20 respectively). The opening time for each injection was set to 10 ms, at a frequency of 0.2 Hz. Each experiment consisted of a 20 min injection set for a total of 240 pulses, before which the chamber was pumped down to a residual pressure of about 10^{-4} Pa. All experiments were carried out in an oxygen atmosphere of 0.44 Pa. During the experiments, the silicon substrate receiving the liquid injections was either left untouched (control sample), heated to 100 °C, exposed to a 300 W oxygen plasma, or both heated and exposed to the plasma. All droplet imprints were then hand-counted on optical micrographs in ImageJ.

3. Results and discussion

The physical aspect of droplet imprints observed on the Si samples varied greatly, even for a given set of injection conditions, and appeared to be first and foremost size-dependent. Therefore, imprints were categorized in basic size classes and their morphology were compared across samples within the same class. Figure 3 shows typical evaporation patterns measured on the control sample (ambient temperature, no plasma), and a sample heated to 100 °C during liquid injection (no plasma either). Although less visible for smaller droplets, imprints on the control sample exhibit quite similar morphologies, regardless of their diameter: a strong, well-defined outer ring and dendrite-like patterns on the inside.

These fractal shapes were never seen under misty plasma deposition conditions. On the other hand, coffee ring shapes shown in Fig. 1 are very similar to what was observed here on the heated sample (Fig 3, second row). Larger drops produced multi-ring structures with an opaque central spot, which is characteristic of the so-called 'stick-slip' motion during evaporation [4]. For the smaller droplets, asymmetric braided shapes and eye-like imprints are also encountered again.

In the experimental conditions chosen for this study, the presence of an oxygen plasma during liquid injection did not have any noticeable effect on the droplet's patterns morphology. Since the samples examined in Fig. 1 were not independently heated, we can conclude that the patterns of Fig. 1 are mostly due to heat brought by the oxygen plasma to the substrate. Indeed, in the latter conditions, sample temperature was measured on the order of 100 °C. On a side note, given the relatively large droplet imprints (> 500 µm for the biggest), an existent but more modest effect of the plasma on droplet morphology could have remained undetected due to the potentially overly abundant quantity of liquid in each pulse. We plan to repeat the experiment using opening times shorter than 10 ms in order to confirm or refute this hypothesis.

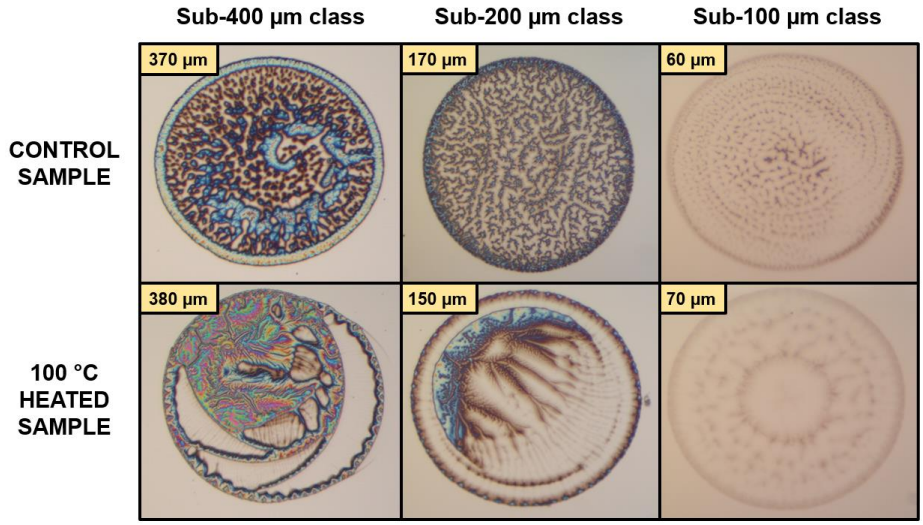

Figure 3 – Optical micrographs of droplet imprints of various size observed on the control sample and the heated sample. Approximate diameters are indicated for each ring structure.

Although no clear impact was detected for droplet morphology, the samples exposed to an oxygen plasma during liquid injection displayed distinct droplet size distributions. Figure 4a shows the size distributions of droplets measured on the control sample and the sample exposed to plasma. No heat was applied to either of these samples. Somewhat surprisingly, the average droplet diameter is larger when the plasma is involved: 280 µm compared to 170 µm for the control sample. However the distributions appear very similar, except that the smallest droplets are much fewer in number when the plasma is on. This suggests a plasma-specific phenomenon, as a purely thermal effect would have led to a full shift of the distribution towards smaller diameters. Moreover, the reduced small-droplet count in plasma conditions is also observed when the sample is heated, as seen in Fig. 4b.

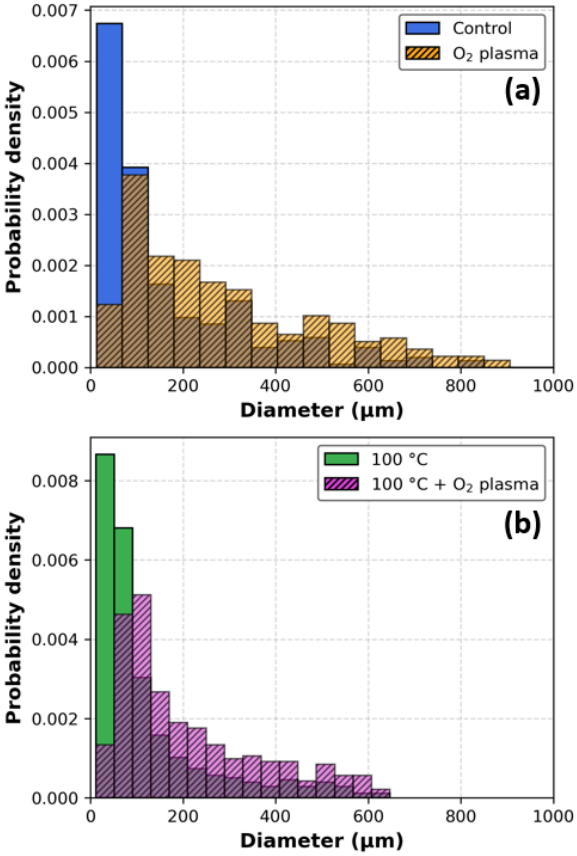

Figure 4 – Droplet size distribution with and without plasma treatment for (a) unheated and (b) heated samples.

A possible explanation for this decrease in the small droplets population could be due to electrostatic charging in the plasma. According to orbital motion limited (OML) theory, droplets promptly acquire a negative charge when immersed in the plasma. Since the sample holder is left at the (negative) floating potential, the competition between the droplet's inertia and electrostatic charge could act as a filter for smaller (i.e. lighter) droplets. This interpretation would be consistent with the RBS results presented thereafter.

Figure 5a shows an *in plasma* RBS spectrum of misty plasma-deposited TiO_2 nanoparticles on a silicon substrate. The Si substrate is clearly visible, as well as a slight contribution of oxygen around 1100 keV. The titanium band is asymmetric, which indicates that the Ti content is not homogeneously distributed but rather more important at the extreme surface. On Figure 5b, the area of this Ti band was extracted as a function of time during liquid injection where the sample was successively exposed to the plasma, heated to 200 °C, and then both exposed to the plasma and heated to 200 °C.

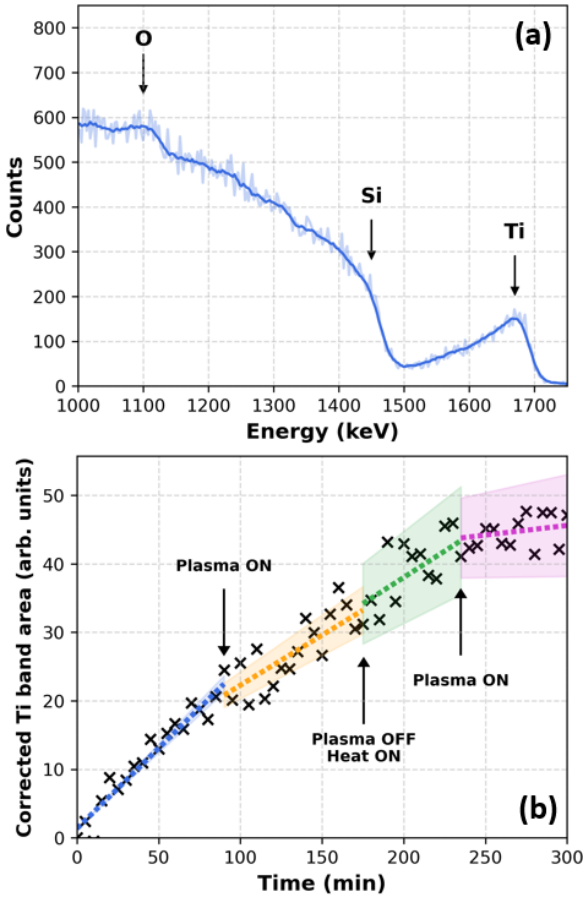

Figure 5 – (a) *In situ* acquired RBS spectrum of TiO_2 nanoparticles on a silicon substrate. (b) Ti content as a function of time during a misty plasma experiment, and corresponding slopes in desposition conditions.

As expected, Ti content increased steadily during the first part of the experiment while TiO_2 nanoparticles were supplied to the sample. A slight change in slope can be seen in Fig 5b after the plasma is turned on. This observation is consistent with the explanation given above for the lack of small droplets on samples exposed to the plasma during liquid injection: if small droplets are repelled by the negative floating potential, part of the Ti content is lost. The slope is also slightly flatter when the sample is heated,

which accounts for the facilitated evaporation of the solvents at higher temperatures. In these conditions, some droplets are fully evaporated before they even reach the sample, and nanoparticles are lost in the vacuum chamber. When both the plasma and sample heating are turned on, these effects combine and the slope becomes even flatter (although still positive). These results also highlight the existing compromise of when it comes to droplet size in misty plasma processes, between small droplets allowing for limited nanoparticle clustering, and large droplets allowing for high-input nanoparticle deposition.

4. Conclusion

In this work, nanoparticle input in low-pressure misty plasma processes was studied in terms of both form and quantity. Coffee ring shape morphology showed a strong dependence on substrate temperature, with thick outer rings and fractal-like central deposits at ambient temperature, as opposed to stick-slip-induced multiring structures at 100 °C. The main reported plasma-specific phenomenon related to droplet size. Samples exposed to an oxygen plasma during liquid injection exhibited size distributions truncated of the smaller diameters, which was ascribed to electrostatic repulsion due to the substrate's negative floating potential. *In situ* RBS analysis confirmed the reduced nanoparticle supply in high-temperature and/or plasma conditions.

5. Acknowledgements

This France-Québec collaboration was carried out as part of the International Research Network on Nanomatériaux Multifunctionnels Contrôlés, supported among others by the CNRS and Nantes Université in France, and Université de Montréal in Québec.

6. References

[1] Mitronika M, Granier A, Goullet A and Richard-Plouet M 2021 Hybrid approaches coupling sol–gel and plasma for the deposition of oxide-based nanocomposite thin films: a review *SN Appl. Sci.* **3** 665

[2] Mitronika M, Profili J, Goullet A, Gautier N, Stephant N, Stafford L, Granier A and Richard-Plouet M 2021 TiO_2–SiO_2 nanocomposite thin films deposited by direct liquid injection of colloidal solution in an O_2/HMDSO low-pressure plasma *J. Phys. D: Appl. Phys.* **54** 085206

[3] Chouteau S, Mitronika M, Goullet A, Richard-Plouet M, Stafford L and Granier A 2022 Kinetics driving nanocomposite thin-film deposition in low-pressure misty plasma processes *J. Phys. D: Appl. Phys.* **55** 505303

[4] Moffat J R, Sefiane K and Shanahan M E R 2009 Effect of TiO_2 Nanoparticles on Contact Line Stick−Slip Behavior of Volatile Drops *J. Phys. Chem. B* **113** 8860–6